Catalysis Today 149 (2010) 288–294

Contents lists available at ScienceDirect

Catalysis Today

journal homepage: www.elsevier.com/locate/cattod

Effect of Ni promoter in the oxide precursors of $MoS_2/MgO–Al_2O_3$ catalysts tested in dibenzothiophene hydrodesulphurization

Alfredo Guevara-Lara [a,*], Alida E. Cruz-Pérez [a], Zeferino Contreras-Valdez [a], Julio Mogica-Betancourt [a], Alejandro Alvarez-Hernández [a], Michel Vrinat [b]

[a] Centro de Investigaciones Químicas, Universidad Autónoma del Estado de Hidalgo, Carr. Pachuca-Tulancingo Km. 4.5, Ciudad Universitaria, Pachuca, Hidalgo, C.P. 42184, Mexico
[b] Institut de Recherches sur la Catalyse et de l'Environnent de Lyon, CNRS, 2 Avenue Albert Einstein, 69626 Villeurbanne Cedex, France

ARTICLE INFO

Article history:
Available online 31 October 2009

Keywords:
Ni promoter effect
Support effect
$MgO–Al_2O_3$, Dibenzothiophene hydrodesulphurization

ABSTRACT

NiMoS catalysts supported on $MgO–Al_2O_3$ oxides, with 95 and 80 mol% of MgO, were synthesized by sol–gel method. In order to study the Ni promoter effect, $MgO–Al_2O_3$ supports were impregnated with a pH = 9 solution of Mo and Ni–Mo, respectively; the catalysts were dried (D) and calcinated (C). Catalytic tests showed a Ni promoter effect of 4.5 on the NiMoMg95Al5-D catalyst and 8.5 on the calcinated one. The latter catalyst is more active than a commercial $NiMo/Al_2O_3$ catalyst. On the other side, the catalyst supported on Mg80Al20 solid did not show any Ni promoter effect. Raman and UV–vis diffuse reflectance spectroscopy showed that during the impregnation step, a strong support interaction with the ion MoO_4^{2-} takes place on the $Mo/MgO–Al_2O_3$ solids. After calcination, MoO_4^{2-} ion remained on the catalyst surface, but increased its interaction with the support. The presence of Ni^{2+}_{Th}, Ni^{2+}_{Oh} and MoO_4^{2-} ions on dried NiMo/Mg95Al5 catalysts was confirmed, as well as the presence of Ni^{2+}_{Th}, Ni^{2+}_{Oh}, MoO_4^{2-} and $Mo_7O_{24}^{6-}$ ions on the calcinated catalyst. This suggests that Ni^{2+} ion allows polymerization of MoO_4^{2-} to $Mo_7O_{24}^{6-}$, produced by $Ni^{2+}_{Oh}–MoO_4^{2-}$ and $Ni^{2+}_{Oh}–Mo_7O_{24}^{6-}$ close interactions. The NiMo/Mg80Al20 solids also showed MoO_3 species and a high Ni^{2+}_{Th} concentration. Thus, the Ni promoter effect and therefore, catalytic activity decreased, due to the formation of Ni^{2+}_{Th}–MgO and $Ni^{2+}_{Th}–Al_2O_3$ spinels.

1. Introduction

In order to obtain 50 ppm weight of sulphur in gasoline and diesel fuels, hydrotreating processes require new catalysts with high activity in hydrodesulphuration of refractory sulphur compounds such as dibenzothiophene and dimethyl-dibenzothiophene [1]. Modification of hydrodesulphurization catalysts by incorporation of acid supports has been performed [2]. Acid supports allow adsorption of sulphur species, but they also promote hydrogenation by protonation followed by hydride transfer. Acid solids can also perform β-DBTs isomerization, and thus, they can increase the rate of hydrodesulphurization [3]. However, acid catalysts can be poisoned by coke [4,5] and, by organic-nitrogen compounds present in gasoline and diesel fuels [6]. On the other side, basic supports allow a high and stable dispersion of catalytically active Mo oxide species. Besides, a basic support could inhibit coke formation [7] Chary et al. [8] reported that MoS_2 supported on MgO is more active in dibenzothiophene (DBT) hydrodesulphurization (HDS) than when it is supported on Al_2O_3, the enhanced activity attributed to high Mo dispersion on MgO support. Pei-Hsin et al. [9] reported the activity of $CoO–MoO_3$ supported on MgO in the HDS of naphtha (gasoline and diesel composition) with initial 0.19% (w/w) of sulphur. This catalyst removes 92% of sulphur and decreases by 0.9 the octane number. This activity remains constant during 408 h of reaction. However, activation by sulphidation (H_2S/H_2) requires more than 20 h. These works do not report a Co or Ni promoter effect. In order to improve MgO properties, Klimova et al. [10] reported a series of sol–gel $MgO–Al_2O_3(x)$ mixed oxides with molar concentrations of x = 0.0, 0.05, 0.25, 0.50, 0.75 and 1 which were successively impregnated with aqueous $(NH_4)_6Mo_7O_{24}$ and $Ni(NO_3)_2$ solutions and then calcinated at 550 °C. These workers reported that the MoS_2 catalyst for thiophene HDS is more active when supported on Al_2O_3 than the complete $MgO–Al_2O_3(x)$ series. The Ni addition to $MoS_2/MgO–Al_2O_3(x)$ catalysts at a Ni/(Ni + Mo) = 0.3 M ratio does not present the Ni–Mo synergy effect. Then, $NiMo/MgO–Al_2O_3(x)$ activity was fivefold lower than $NiMo/Al_2O_3$ catalyst. The Ni–Mo synergy effect was obtained with a Ni/(Ni + Mo) = 0.6 M ratio. However, activity was only 50% of that observed with $NiMo/Al_2O_3$ catalyst. These

* Corresponding author. Tel.: +52 77 17 17 20 00x2202; fax: +52 77 17 17 20 00x6502.
E-mail address: guevaraa@uaeh.edu.mx (A. Guevara-Lara).

0920-5861/$ – see front matter © 2009 Elsevier B.V. All rights reserved.
doi:10.1016/j.cattod.2009.09.014

authors suggest that Ni incorporates into support with the formation of a solid NiO–MgO solution. Additionally, in their study of hydrotreatment catalysts supported on Al_2O_3–MgO, Houssenbay et al. [11] reported that during aqueous Mo impregnation, the $MgMoO_4$ spinel is formed, which is dissolved during aqueous Ni impregnation ($MgMoO_4$ solubility is 14 g/100 ml of water at 22 °C).

Aqueous impregnation of Ni and Mo on MgO presents serious problems, the high MgO surface area allows a reaction with water and $Mg(OH)_2$ formation [12]. The pH = 5.2–5.5 of an aqueous $(NH_4)_6Mo_7O_{24}$ and $Ni(NO_3)_2$ solution and net surface pH = 12 of MgO contribute to the MgO → $Mg(OH)_2$ transformation. In order to solve this problem, Zdražil et al. [13–15] propose the use of organic solvents such as dimethylsulphoxide and methanol. It seems that the superficial MgO texture is stable with these solvents. However, $(NH_4)_6Mo_7O_{24}$ and $Ni(NO_3)_2$ solubility in these solvents is low and consequently, the dispersion is low too. Preceding studies suggest the study of hydrotreatment catalysts modified with basic MgO supports that decrease coke formation and hydrogen consumption. Furthermore, during their preparation these modified catalysts will prevent NiMgO and $MoMgO_4$ formation.

The aim of this work is to show that, by means of preparation methods, the Ni promoter effect of MoS_2/MgO–Al_2O_3 catalysts can be improved. Therefore, we present a systematic study of superficial Ni and Mo species during the preparation of NiMo/MgO–Al_2O_3 catalysts.

2. Experimentation

2.1. MgO–Al_2O_3 support preparation

MgO–Al_2O_3 supports were prepared by sol–gel method [10]. Magnesium ethoxide was dissolved in 1-propanol (1 g ethoxide/100 mol alcohol), and then stirred during 12 h. Next, aluminum isopropoxide was added, and then stirred for 12 h. The gel was obtained by hydrolysis with dropwise addition of deionized water. Then, the gel was dried at 100 °C for 24 h and then calcinated at 550 °C (5 °C/min) for 6 h. The names of supports: Mg80Al20 and Mg95Al5 stand for 20 mol% and 5 mol% Al_2O_3, respectively.

2.2. Preparation of Mo/MgO–Al_2O_3 and NiMo/MgO–Al_2O_3 catalysts

Supports, crushed and sieved (100–150 mesh), were co-impregnated with an aqueous $(NH_4)_6MoO_7{\cdot}6H_2O$ + $Ni(NO_3)_2{\cdot}6H_2O$ solution in order to get a concentration of 12 wt.% of MoO_3 and 3 wt.% of NiO using the incipient wetness impregnation technique. In order to have an impregnation solution with MoO_4^{2-} and $[Ni^{2+}4O^{2-}]$ species, the pH solution was adjusted to 9, by the addition of a 0.01 M NH_4OH solution. These solids were kept at room temperature for 24 h and then dried at 110 °C for 4 h. Solids obtained are named: MoMg95Al5 and NiMoMg95Al. Letters, D and C were added to indicate dried and calcinated catalysts, respectively.

2.3. Catalyst characterization

MgO–Al_2O_3 supports were characterized by N_2 physisorption, X-rays diffraction (XRD) and ζ-potential. N_2 physisorption was performed on an ASAP 2020 Micromeritics apparatus. Specific surface area and porous size were calculated by application of the Brunauer, Emmet and Teller (BET) and BJH desorption isotherm models, respectively. Before measurement, dried samples were treated at 180 °C for 12 h under vacuum at $P = 80 \times 10^{-6}$ mmHg. Calcinated samples were treated at 300 °C during 4 h under vacuum at $P = 30 \times 10^{-6}$ mmHg. XRD measurements were performed with a Phillips diffractometer using CuKα radiation (λ = 1.5418 Å) in a $15° < 2\theta < 80°$ (2°/min) range. ζ-Potential values were measured using a Malvern ZetaSizer 3000 apparatus; 0.05 g of support/L was dispersed as a colloidal suspension in 1×10^{-2} mol of KNO_3/L aqueous solution at 25 °C. Catalysts in oxidized state were characterized by Raman and UV–vis diffuse reflectance (UV–vis DRS) spectroscopies. Raman spectra were recorded on a PerkinElmer GX Raman FT-IR apparatus equipped with a Nd:YAG (1064 nm) laser and an InGaAs detector. For each spectrum, an average of 10–50 scans were obtained with a laser power of 40–300 mW in the 1500–100 cm^{-1} range, with a resolution of 2–4 cm^{-1}. UV–vis diffuse reflectance spectra (UV–vis DRS) were recorded on a PerkinElmer Lambda 40 spectrometer equipped with an integration sphere. As reference for UV–vis DRS, we used the Spectralon SRS-99-010 (99% reflectance) tablet. In the recording of the reflectance data shown, the Kubelka–Munk ($F(R_\infty)$) function was applied:

$$F(R_\infty) = \frac{(1 - R_\infty)^2}{2R_\infty} \quad (1)$$

in which R_∞ is the reflectance at infinite depth.

2.4. Catalytic tests

Catalysts were activated by sulphidation with a flow of 4 L/h of a 10 mol% H_2S/H_2 gas mixture at 400 °C (5 °C/min) during 4 h. Catalysts were tested in the hydrodesulphurization of a model of gasoline (a mixture of dibenzothiophene and n-heptane). Tests were carried out in a continuous flow trickle-bed micro-reactor with 0.05 g of catalyst at $T = 300$ °C and $P = 30$ bar. The reactor was fed with a flow of 1.2×10^{-4} L/h (STP) of a solution of 0.37 mol of DBT in n-heptane and a flow of 2.2 L/h of H_2 (STP). n-Dodecane was added to the liquid feed as an internal standard for gas chromatography, in the same molar amount as DBT. N-heptane was selected as solvent because under the reaction conditions: $T = 300$ °C and $P = 30$ bar, all reactants are in gas phase [16]. Liquid samples were analyzed by gas chromatography on a PerkinElmer AutoSystem instrument equipped with a FID detector and a HP-Ultra 2 (30 m × 0.32 mm i.d.) column. Main reaction products were biphenyl and cyclohexylbenzene. Reaction rates were calculated considering first order kinetics and a differential reactor as follows:

$$r_i = \frac{F_{i_0} x_i}{m_c} \quad (2)$$

where F_{i_0} = feed molar flow of DBT, m_c = weight of catalyst, x_i = DBT conversion.

$$x_{DBT} = \frac{C_{DBT_0} - C_{DBT}}{C_{DBT_0}} = \frac{\sum A_i}{\sum A_i + A_{DBT}} \quad (3)$$

where A_i = peak area of i products in the chromatogram.

3. Results and discussion

3.1. Effect of Al_2O_3 concentration on MgO structure

X-ray powder diffraction of MgO–Al_2O_3 supports is shown in Fig. 1. Mg95Al5 support shows 2θ = 42.9, 62.3, 78.7 and 74.7 peaks, which are associated to periclase MgO cubic structure, 450946 PDF-File. In addition, at 2θ = 36.8 peak is observed, which corresponds to the $MgAl_2O_4$ spinel (211152 PDF-file). Mg80Al20 diffractogram (amplify 2×) shows wider, less intense peaks of MgO periclase and $MgAl_2O_4$ spinel. Besides, it also shows at 2θ = 11.4, 23 and 34.9 peaks, which correspond to $MgAl(OH)_{14}{\cdot}H_2O$ structure (430072 PDF-file). Similar effects of Al_2O_3 concentration on MgO structure has been observed on MgO–Al_2O_3 solids prepared by sol–gel [10] and precipitation [17] methods and on solids obtained from hydrotalcites [18].

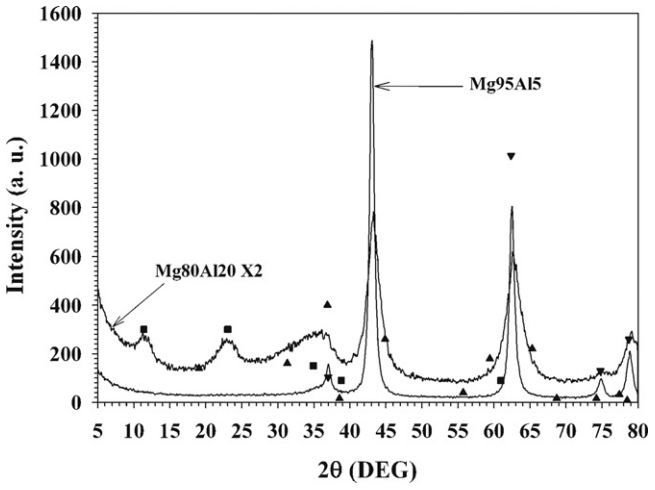

Fig. 1. X-rays diffraction of MgO–Al_2O_3 supports. Calcinated at $T = 500$ °C. (▼) = MgO periclase, (▲) = $MgAl_2O_4$ spinel, and (◆) = $MgAl(OH)_{14}{\cdot}H_2O$.

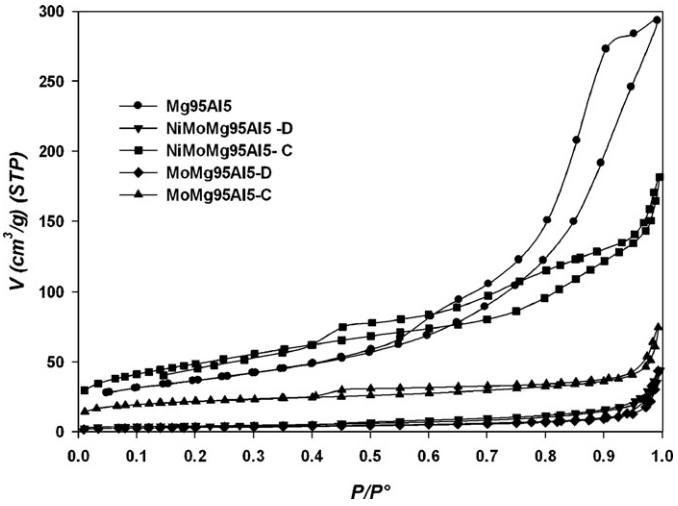

Fig. 2. N_2 adsorption–desorption isotherms of Mo and NiMo supported on Mg95Al5.

3.2. Effect of Al_2O_3 concentration on MgO texture

Fig. 2 shows N_2 adsorption–desorption isotherms of Mo and NiMo supported Mg95Al5. Mg95Al5 isotherm corresponds to type II isotherm and type H1 hysteresis which are characteristic of macroporous solids consisting of particles crossed by nearly cylindrical channels or agglomerates of spheroidal particles with uniform size and shape [19]. After Mo and Ni–Mo impregnation, NiMoMg95Al5-D and MoMg95Al5-D showed similar isotherms. However, the low degasification temperature, suggests that adsorbed water is not completely eliminated and thus no conclusion can be drawn from these results.

The isotherm of calcinated MoMg95Al5-C shows that Mo-support interaction modified the support texture. However, Ni addition allows the support to maintain its texture and specific surface, Table 1, as it is showed by the NiMoMg95Al5-C isotherm. This is likely due to a better Ni–Mo interaction. Mg80Al20 support presents type II isotherm and type H2 hysteresis, Fig. 3, which is similar to Mg95Al5 support but without uniform size and shape. NiMoMg80Al20 isotherm is different from Mg80Al20 isotherm, it suggests a modification of support texture; probably due to Ni-support and Mo-support interactions. However, specific surface, does not decrease as it is observed with the MoMg80Al20 solid (Table 1).

Table 1
Results of N_2 physisorption of NiO–MoO_3/MgO–Al_2O_3 solids.

Solid	A_{BET} (m^2/g)	V_P (cm^3/g)	Porous size (nm)
Mg95lA5	140	0.45	14
MoMg95Al5-D	10	0.03	12
MoMg95Al5-C	77	0.07	4
NiMoMg95Al5-D	15	0.04	8
NiMoMg95Al5-C	166	0.23	3
Mg80Al20	197	0.36	7
MoMg80Al20-D	23	0.9	12
NiMoMg80Al20-D	20	0.1	9
NiMoMg80Al20-C	136	0.2	4

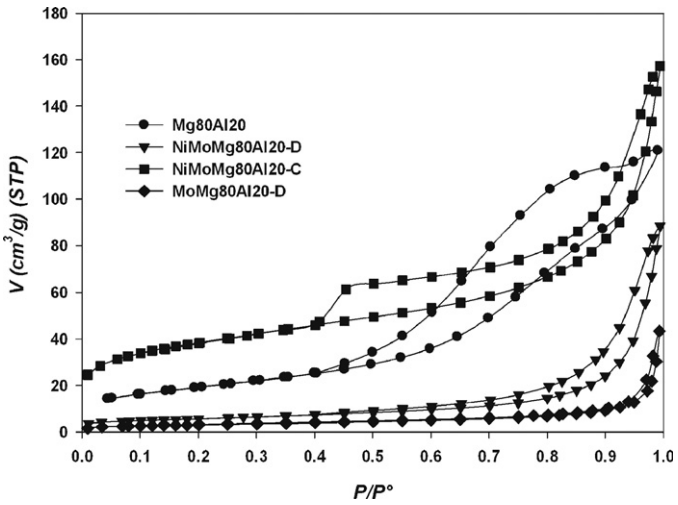

Fig. 3. N_2 adsorption–desorption isotherms of Mo and NiMo supported on Mg80Al20.

Table 1 shows that specific surface area increases with Al_2O_3 content. Textural properties of MgO–Al_2O_3 supports prepared by sol–gel method are better than those reported for solids obtained by the precipitation method [17] and from hydrotalcites [18]. These results are similar to those reported by Klimova et al. [10].

3.3. Effect of Al_2O_3 concentration on MgO superficial charge: ζ-potential

Mg95Al5 and Mg80Al20 supports present similar ζ-potential curves, Fig. 4. This suggests that these solids have similar superficial charges, since both solids present the periclase structure. ζ-Potential is stable between pH = 2 and 3.7 and increases at pH = 4.5. This increase could be associated to the

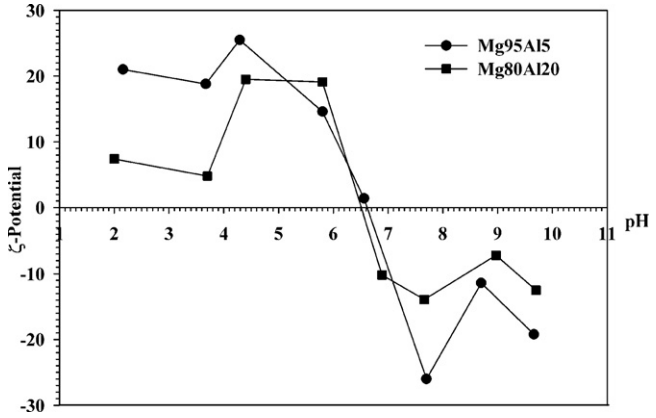

Fig. 4. ζ-Potential of MgO–Al_2O_3 colloidal solutions as a function of pH. $T = 25$ °C.

Table 2
Dibenzothiophene hydrodesulphurization.

Catalysts	r ($\times 10^{-7}$ mol s^{-1} gCata^{-1})	Selectivity (%)	
		Byphenil	CHB
MoSMg95Al5-D	5	66.4	33.6
MoSMg95Al5-C	3	85.6	14.4
NiMoSMg95Al5-D	21	98.0	2.0
NiMoSMg95Al5-C	26	95.7	4.3
NiMoSMg80Al20-D	7	98.0	2.0
NiMoSMg80Al20-C	6	98.0	2.0
NiMoS/Al_2O_3 (commercial)	24	95.5	4.5

T = 300 K and P = 30 bar.

MgO → $Mg(OH)_2$ transformation [12]. In the range of pH = 4.2–6.5, ζ-potential decrease proportionally to pH increase. This suggests adsorption of OH^- on the surface, until the surface is negatively charged. Then, it suggests that with solutions of pH < 5, MgO is transformed to $Mg(OH)_2$. Furthermore, Mg95Al5 and Mg80Al20 will be stable in contact with basic solutions. In order to prevent MgO dissolution, pH solution was adjusted to major values of iso-electric point of MgO–Al_2O_3 supports. ζ-Potential method is based on the assumption that when an oxide is placed in a solution with a pH similar to its iso-electric point (IEP), there will be no change in the pH solution. IEP is obtained from the intersection of ζ-potential curve on pH axis, this point is named: point of zero charge (PZC). Then, IEP or PZC are associated to net surface pH of the oxide [20]. Fig. 4 shows the supports present a net surface pH = 6.5. This value is very different from the pH = 12 reported for the periclase MgO [21] which suggests a modification of MgO superficial charges due to the addition of Al_2O_3. Bolognini et al. [18] reported CO_2 desorption programmed temperature of MgO–Al_2O_3 solids, these authors show that the basicity of solids decreases as the Mg content increases.

3.4. Catalytic evaluation of NiMoS/MgO–Al_2O_3 catalysts

In order to study the Ni promoter effect on MoS_2/MgO–Al_2O_3 catalysts, MgO–Al_2O_3 supports were impregnated with Mo and NiMo. The strong interaction of Mo–MgO and Ni–MgO prompts the study of Ni and Mo species during impregnation and calcination steps and their effect on catalytic activity. Catalytic evaluation results of dried and calcinated catalysts are summarized in Table 2. MoSMg95Al5-D is more active than the MoSMg95Al5-C catalyst. This suggests that calcination step decreased the MoS_2 catalytic activity. For comparison the Ni promotor effect is defined as NiPE = r_{NiMo}/r_{Mo} (NiMo catalyst rate/Mo catalyst rate). NiMoSMg95Al5-D catalyst shows a NiPE = 4.2 whereas NiMoSMg95Al5-C catalyst a NiPE = 8.5. These results suggest that impregnation with a pH = 9 solution allows a natural promoter effect of Ni. However, Ni promoter effect is also associated with the composition of support. NiMoSMg80Al20-D and NiMoSMg80Al20-C catalysts present an activity similar to MoSMg95Al5 catalyst. In this case, the promoter effect of Ni is not observed. As a reference for catalytic activity, a commercial NiMoS/Al_2O_3 was tested. The catalyst series showed the following order: NiMoSMg95Al5-C > NiMoS/Al_2O_3 > NiMoSMg95Al5-D > NiMoMg80Al20-D > NiMoMg95Al5-C. NiMoSMg95Al5-C is more active than NiMo/Al_2O_3 catalyst.

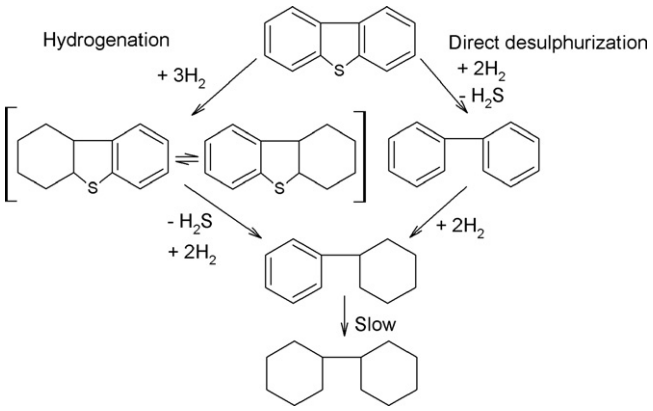

Fig. 5. Reaction network of dibenzothiophene hydrodesulphurization proposed by Houlla et al. [22].

In accord to Houlla et al. [22], dibenzothiophene hydrodesulphurization has two reaction paths, Fig. 5, the so-called "direct desulphurization" path in which biphenyl is principally produced and biphenyl hydrogenation to cyclohexylbenzene is comparatively slow; and, the so-called: "hydrogenation" path in which 1,2,3,4-tetrahydrodibenzothiophene and 1,2,3,4,5,6-hexahydrodibenzothiophene are produced and are rapidly converted to cyclohexylbenzene.

MoSMg95Al5-D catalyst shows a selectivity for biphenyl of 66.4%, and after calcination the selectivity increase to 85%, Table 2. 95% biphenyl selectivity of NiMoS supported on MgO–Al_2O_3 catalysts suggest that these catalysts prefer the direct desulphurization path in which it is consumed a comparatively low quantity of H_2.

These results suggest that pH impregnation solution, support composition and calcination have a direct effect on the activity of catalysts supported on MgO–Al_2O_3. Therefore, Mo and Ni molecular species supported on Mg95Al5 and Mg80Al20 will be studied during the impregnation and calcination steps.

3.5. Effect of support composition on Ni and Mo species supported on MgO–Al_2O_3

3.5.1. Raman and absorbance UV–vis spectroscopy of impregnation solutions

Molybdenum and nickel species in impregnation solution could be associated to impregnated species on support [23–25]. Table 3 summarizes the Ni and Mo species observed in Raman [26–29] and UV–vis absorbance spectra of aqueous $(NH_4)_6Mo_7O_7{\cdot}6H_2O$ + $Ni(NO_3)_2{\cdot}6H_2O$ impregnation solution at pH = 9 and 6. Raman spectrum of pH = 9 solution showed mainly the MoO_4^{2-} ion whereas at pH = 6 it showed the $Mo_7O_{24}^{6-}$ ion. For nickel species, Raman spectra [29] would show a ~400 cm^{-1} band of $Ni(OH)_2$ species at pH = 9 and a 490 cm^{-1} band at pH = 6 corresponding to $Ni_4(OH)_4^{4+}$. However, the low nickel concentration does not allow a good assignation of Raman shifts. Raman spectra show a 1050 cm^{-1} band, which corresponds to the N–O stretching vibration of NO_3^- ions, from $Ni(NO_3)_2$ salt.

UV–vis absorbance spectroscopy allows the study of Mo(IV) ions due to its d° electronic configuration. The spectrum is

Table 3
Summary of Mo and Ni species observed in aqueous $(NH_4)_6Mo_7O_{24}{\cdot}4H_2O + Ni(NO_3)_2$ solution.

	$Mo_7O_{24}^{6-}$	MoO_4^{2-}	$[Ni(H_2O)_6]^{2+}$	$[Ni^{2+}4O^{2-}]$	$[Ni^{2+}6O^{2-}]$	$(NO_3)^{2-}$
Raman (cm^{-1})	945, 240, 210	897, 370, 300, 312				1050
Absorbance UV–vis (nm)			393	623, 650	710, 736, 973	220

pH = 6 and 7. T = 25 °C and P = 1 atm.

produced by a $O^{2-} \rightarrow Mo^{6+}$ charge transfer. This band is observed between 200 and 400 nm. Electronic transition energy depends on the symmetry of ligand field around the Mo center. For oxo-ligands, the transition energy is higher for tetrahedral than for octahedral Mo(IV) ion [30]. For Ni^{2+} [31–33], solutions at pH = 6 and 9 show $[Ni^{2+}4O^{2-}]$ and $[Ni^{2+}6O^{2-}]$ species, which correspond to tetrahedral and octahedral Ni^{2+} ions, respectively. Solution of pH = 6 shows $[Ni^{2+}4O^{2-}]$ and $[Ni^{2+}6O^{2-}]$ bands with similar intensity. Since these spin transitions are allowed, they suggest a similar concentration of $[Ni^{2+}4O^{2-}]$ and $[Ni^{2+}6O^{2-}]$ species. For pH = 9 solution, the 623 nm band is more intense than the 730 nm band, suggesting a high concentration of $[Ni^{2+}4O^{2-}]$ species.

In order to obtain a better Mo and Ni dispersion, pH impregnation solution was adjusted to 9. Ni and Mo bands could be displaced due to interactions between Ni–Mo, NiMo-support, Mo-support and Ni-support which cause a distortion in local Mo and Ni symmetry.

3.5.2. Mo/MgO–Al_2O_3 catalysts

UV–vis diffuse reflectance spectrum (UV–vis DRS) of a MoMg95Al5-D solid show a 242 nm band, Fig. 6. On the other hand, MoMg95Al5-C catalyst presents a band at 239 nm. These bands are associated to tetrahedral Mo(IV). This displacement is probably due to the strong Mo-support interaction, caused by calcination. MoMg80Al20-D and -C solids present 244 nm and 256 nm bands, respectively, which are associated to tetrahedral Mo(IV). In this case, this displacement could be associated to a low Mo-support interaction.

Raman spectra of Mo/MgO–Al_2O_3 are showed in Fig. 7. MoMg95Al5-D solid presents 908 and 315 cm^{-1} Raman shifts which are associated to MoO_4^{2-} ion. In solution, this ion presents a band at 897 cm^{-1}. This displacement is attributed to the Mo-support interaction. The band at 203 cm^{-1} is associated to $Mo_7O_{24}^{6-}$ ion with Mo–O–Mo vibration modes. The 445 cm^{-1} band is associated to stretching (A_{1g}) vibration of $Mg(OH)_2$ [34]. This Raman shift suggests that Mg95Al5 solid is not stable during the impregnation step. After calcination, MoMg95Al5-C shows Raman shifts similar to dried solid. These results suggest that the calcination step does not modify the Mo-impregnated species. However, the 912 cm^{-1} shift suggests a strong MoO_4^{2-}-support interaction. In consequence, during activation, sulphidation will be easier on the dried catalyst than on the calcinated solid. Then, the activity in DBT HDS will be higher in the dried catalyst, Table 2.

On the other side, MoMg80Al20-D solid only shows a 203 cm^{-1} Raman band, which is associated to $Mo_7O_{24}^{6-}$ ion with Mo–O–Mo vibration mode. In this case, net surface pH = 6.5 controls the Mo superficial species. However, UV–vis DRS shows MoO_4^{2-} ions. XRD results showed that this solid has periclase MgO and $MgAl(OH)_{14}{\cdot}H_2O$ structures. Then, Mo_4O^{2-}-impregnated would react with M–OH (M = Al, Mg) species. The strong interaction would cause the absence of Mo=O_t Raman vibration modes (830–970 and 890–1000 cm^{-1}) and, it would only show the Mo–O–Mo vibration mode (560 and 210 cm^{-1} Raman shift). The MoMg80Al20-C solid shows bands at 232 and 203 cm^{-1}, which are attributed to $Mo_7O_{24}^{6-}$ ion.

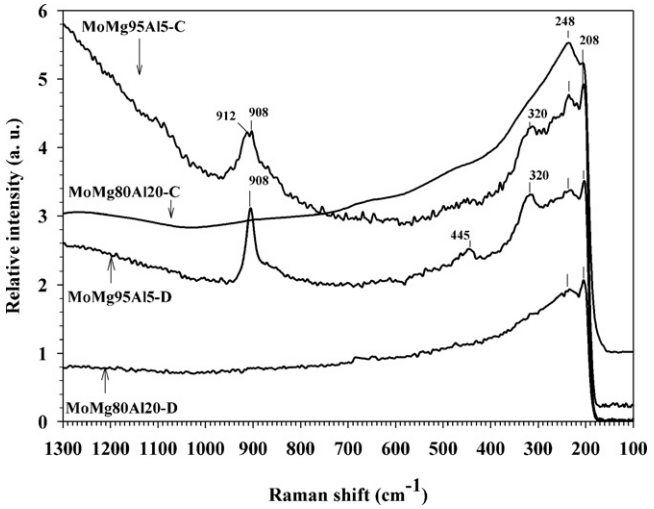

Fig. 7. Raman spectra of Mo/MgO–Al_2O_3 catalysts, dried (D) at T = 120 °C and calcinated (C) at T = 400 °C.

3.5.3. Ni effect

UV–vis diffuse reflectance spectra of NiMo/MgO–Al_2O_3 catalysts, in the 200–400 nm wavelength range are showed in Fig. 8. Nitrate ion, from the $Ni(NO_3)_2$ salt, produces the 220 nm band, which is eliminated during calcination. NiMoMg95Al5-D solid shows a 235 nm band associated with the MoO_4^{2-} ion. After calcination step, NiMoMg95Al5-C shows a wider band that is formed by the 238 and 270 nm bands of MoO_4^{2-} and $Mo_7O_{24}^{6-}$ ions, respectively. NiMoMg80Al20-D solid shows a broad band composed by 238 and 276 nm bands of MoO_4^{2-} and $Mo_7O_{24}^{6-}$ ions, respectively. After calcination process, NiMoMg80Al20-C solid shows a 318 nm band associated to MoO_3. Comparison of

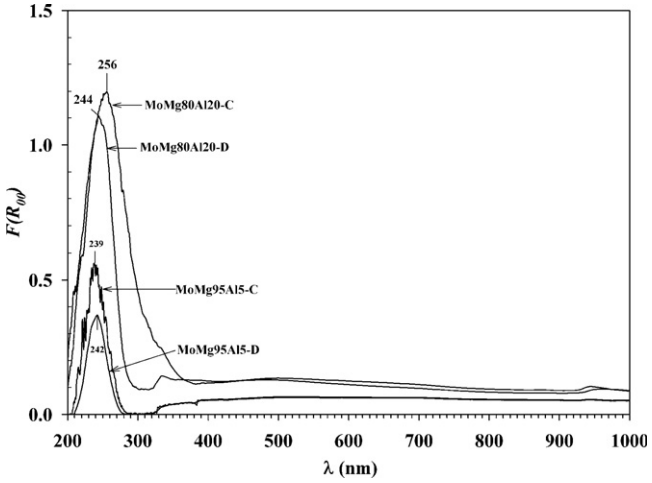

Fig. 6. UV–vis diffuse reflectance spectra of Mo/MgO–Al_2O_3 solids, (D) dried at T = 120 °C and (C) calcinated at T = 400 °C.

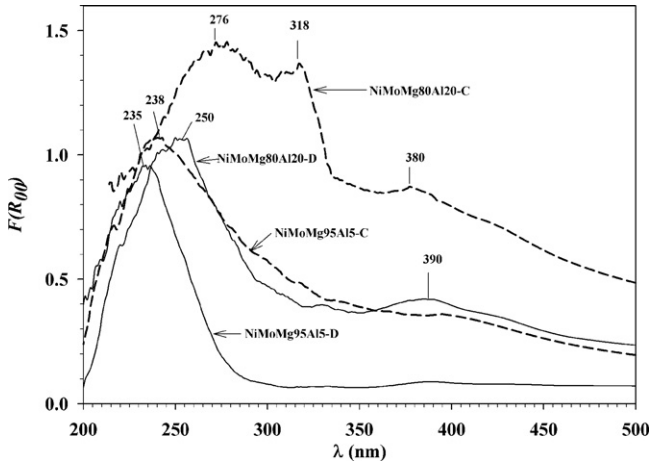

Fig. 8. UV–vis diffuse reflectance spectra of NiMo/MgO–Al_2O_3 solids 200–400 nm wavelength range.

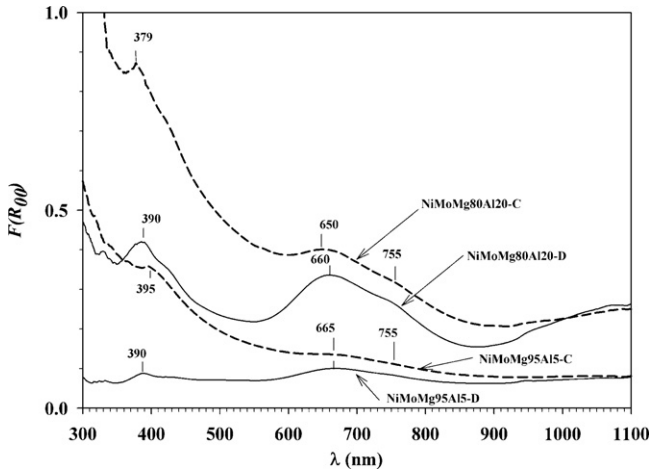

Fig. 9. UV–vis diffuse reflectance spectroscopy of NiMo/MgO–Al_2O_3 in 400–1100 nm wavelength range.

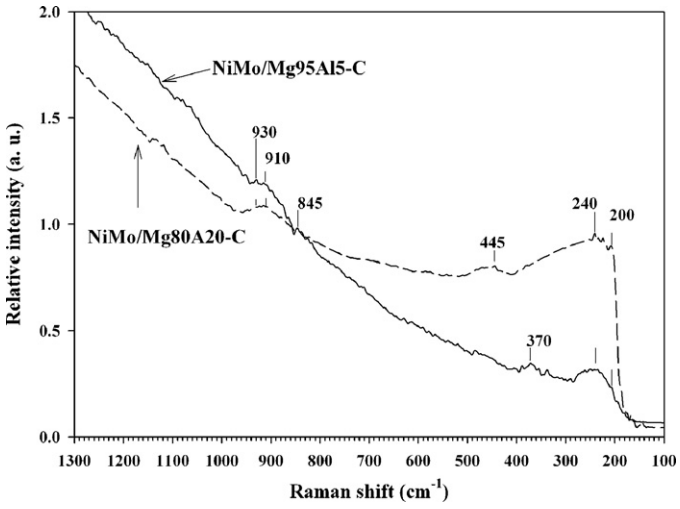

Fig. 11. Raman spectra of calcinated NiMo/MgO–Al_2O_3 solids.

these results with those obtained from Mo/MgO–Al_2O_3 solids suggest that Ni causes the polymerization from MoO_4^{2-} to $Mo_7O_{24}^{6-}$, during calcination. Fig. 9 shows the UV–vis diffuse reflectance spectra of NiMo/MgO–Al_2O_3 solids, impregnated with a pH = 9 solution, in the 400–1100 nm wavelength region. Bands at 390 nm are associated to $[Ni(H_2O)_6]^{2+}$ ion [32,35]. At ~660 nm band is related to Ni^{2+} distorted tetrahedral symmetry $[Ni^{2+}4O^{2-}]$ and the 755 nm band corresponds to Ni^{2+} distorted octahedral symmetry $[Ni^{2+}6O^{2-}]$ [33,36]. NiMoMg95Al5-D and -C solids show bands at 665 and 755 nm with similar intensity, these are associated to tetrahedral and octahedral Ni^{2+}, respectively. Also, NiMoMg80Al20-D and -C solids show similar spectra of $[Ni^{2+}4O^{2-}]$ and $[Ni^{2+}6O^{2-}]$ species.

Fig. 10 shows the Raman spectrum of NiMoMg95Al5-D with bands observed at 1045 cm^{-1} assigned to NO_3^{2-} ion, 906 and 320 cm^{-1} of MoO_4^{2-} ion and 232 and 200 cm^{-1} of $Mo_7O_{24}^{6-}$ ion. These bands are similar to those observed on the Raman spectrum of MoMg95Al5-D. On the contrary, NiMoMg80Al20-D does not show bands, as those observed in the MoMg80Al20 spectrum. The dried solids show bands at 275 and 441 cm^{-1} which are attributed to structural vibration (E_g) and stretching vibration (A_{1g}) of Mg–O from $Mg(OH)_2$. These bands suggest that MgO–Al_2O_3 solids are not stable with a pH basic solution impregnation. After calcination, NiMoMg95Al5-C shows bands at 930 and 240 cm^{-1} corresponding to $Mo_7O_{24}^{6-}$ ion and bands at 910 and 370 cm^{-1} corresponding to

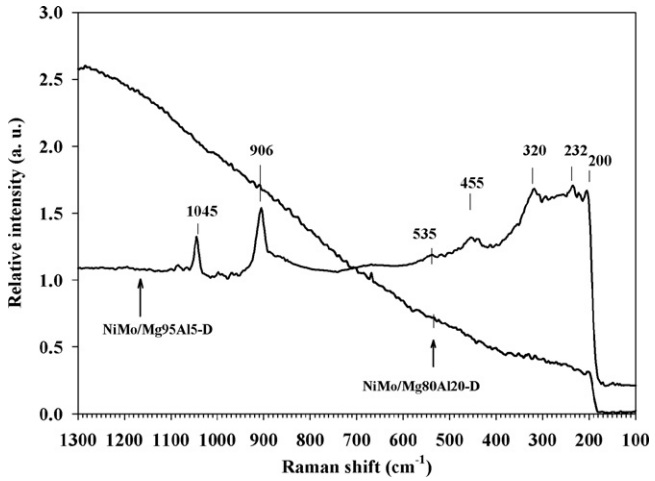

Fig. 10. Raman spectra of dried NiMo/MgO–Al_2O_3 solids.

MoO_4^{2-} ion, Fig. 11. Compared to MoMg95Al5-C, it can be suggested that Ni allows polymerization from MoO_4^{2-} to $Mo_7O_{24}^{6-}$, during calcination. In the case of solid NiMoMg80Al20-C, it shows bands of MoO_4^{2-} and $Mo_7O_{24}^{6-}$ ions, as observed in UV–vis DRS, Fig. 8. These species are not observed in NiMoMg80Al20 or MoMg80Al20 solids. This suggests that Ni does not interact with Mo species. The impregnation solution at pH = 9 contains mainly MoO_4^{2-} and $[Ni^{2+}4O^{2-}]$ species. However, during impregnation, OH^- ions from solution charge negatively the surface: $-M^{\cdot\cdot}OH^-$ and $-MO^-$. Therefore, during impregnation, MoO_4^{2-}, $Mo_7O_{24}^{6-}$ and superficial $-M^{\cdot\cdot}OH^-$ compete for Ni^{2+} species. On one side, Ni and Mo could form $NiMoO_4$ hydroxide clusters with alpha and beta phases. In alfa phase, Mo symmetry is tetrahedral, in beta phase symmetry is octahedral and, Ni is octahedral in both alpha and beta phases [28]. On the other side, Ni^{2+} could directly react with the support to form Ni^{2+}/γ-Al_2O_4 [33,36] or Ni^{2+}/MgO spinels. Ni^{2+} ions mainly have tetrahedral symmetry. XRD results of Mg95Al5 support mainly showed MgO periclase structure. Raman and UV–vis DR spectroscopy showed that this support contains the MoO_4^{2-} ion in combination with $[Ni^{2+}4O^{2-}]$ and $[Ni^{2+}6O^{2-}]$ ions. After calcination, NiMoMg95Al5-C showed the $Mo_7O_{24}^{6-}$ ion. Thus, it can be suggested that Ni allows polymerization from MoO_4^{2-} to $Mo_7O_{24}^{6-}$ during calcination. This polymerization leads to the formation of superficial Ni^{2+}/MoO_4^{2-} and $Ni^{2+}/Mo_7O_{24}^{6-}$ in close interaction. These ions are thus responsible for the Ni promoter effect on MoS_2 catalysts in HDS of DBT, Table 2. XRD results of Mg80Al20 support showed MgO periclase and $MgAl(OH)_{14}\cdot H_2O$ structures. During impregnation, the pH = 9 of solution charged negatively the support surface, then Ni^{2+} reacts strongly with the support, as the UV–vis DRS spectra of NiMoMg80Al20-D and NiMoMg80Al20-C solids show. In these spectra the $[Ni^{2+}4O^{2-}]$ band is more intense than that of $[Ni^{2+}6O^{2-}]$. This suggests that Ni promoter effect is lost as a consequence of strong interaction between Ni and support, which avoids Ni–Mo interaction. This can be observed on the results showed in catalytic evaluation of DBT HDS, Table 2.

4. Conclusions

MgO modified with Al_2O_3 by sol–gel method, allows production of supports with structure and texture suitable for hydrotreatment processes. Raman and UV–vis results showed that during impregnation, there is a strongly Ni- and Mo-support interaction. These interactions become higher with calcination. The high catalytic activity of sulphided NiMo/MgO–Al_2O_3 catalysts in HDS of

DBT was linked to formation of Ni^{2+}/MoO_4^{2+} and $Ni^{2+}/Mo_7O_{24}^{6-}$ species in the oxide precursors, in which Ni^{2+} ions interacted strongly with polymerized molybdenum oxide species.

References

[1] H. Schulz, W. Bohringer, F. Ousmanov, P. Waller, Fuel Process. Technol. 61 (1999) 5–41.
[2] H. Pines, The Chemistry of Catalytic Hydrocarbon Conversions, Academic Press, New York, 1981, pp. 99–100.
[3] T.C. Ho, Catal. Today 98 (2004) 3–18.
[4] E. Furimsky, F.E. Massoth, Catal. Today 52 (1999) 381.
[5] Y.H. Hu, E. Ruckenstein, Catal. Rev. 44 (2002) 423–453.
[6] M. Breysse, P. Afanasiev, C. Geantet, M. Vrinat, Catal. Today 86 (2003) 5–16.
[7] T. Klicpera, M. Zdražil, J. Catal. 206 (2002) 314–320.
[8] K.V.R. Chary, H. Ramakrishna, K.S.R. Rao, G.M. Dhar, P.K. Rao, Catal. Lett. 10 (1991) 27–34.
[9] A. Pei-Hsin Yu, E. C. Myers, Catalysts for Selective Hydrodesulphurization, Standard Oil Company, UK Patent Application GB 2 017 743 A, 10 October 1979.
[10] T. Klimova, D.S. Casados, J. Ramírez, Catal. Today 43 (1998) 135–146.
[11] S. Houssenbay, E. Payen, S. Kasztelan, J. Grimblot, Catal. Today 10 (1991) 541.
[12] J.M.M. Llorente, V. Rives, P. Malet, F.J. Gil-Llambias, J. Catal. 135 (1992) 1–12.
[13] E. Hillerová, Z. Vít, M. Zdražil, Appl. Catal. A 118 (1994) 111.
[14] T. Klicpera, M. Zdražil, Appl. Catal. A 216 (2001) 41.
[15] M. Zdražil, Catal. Today 86 (2003) 151–171.
[16] A. Guevara, R. Bacaud, M. Vrinat, Appl. Catal. A 253 (2003) 515–526.
[17] L. Shuzhi, Z. Bangwei, S. Xiaolin, O. Yifang, X. Haowen, X. Zhongyu, J. Mater. Process. Technol. 89–90 (1999) 405–409.
[18] M. Bolognini, F. Cavani, D. Scagliarini, C. Flego, C. Perego, M. Saba, Catal. Today 75 (2002) 103–111.
[19] G. Leofanti, M. Padovan, G. Tozzola, B. Venturelli, Catal. Today 41 (1998) 207.
[20] J. Hunter, in: R.H. Ottewill, R.L. Rowell (Eds.), Zeta Potential in Colloid Science: Principles and Applications, Colloid Science Series of Academic Press, London, 1981.
[21] A.G. Parks, Chem. Rev. 65 (1965) 177.
[22] M. Houlla, D.H. Broderick, A.V. Sapre, N.K. Nag, V.H.J. de Beer, B.C. Gates, H. Kwart, J. Catal. 61 (1980) 523–527.
[23] H. Hu, S.R. Bare, I.E. Wachs, J. Phys. Chem. 99 (1995) 10910.
[24] G. Deo, I.E. Wachs, J. Phys. Chem. 95 (1991) 5889.
[25] H. Jeziorowski, H. Knözinger, J. Phys. Chem. 83 (1979) 1166.
[26] M.A. Vuurman, I.E. Wachs, J. Phys. Chem. 96 (1992) 5008–5016.
[27] S.C. Chang, M.A. Leugers, S.R. Bare, J. Phys. Chem. 96 (1992) 10358–10365.
[28] J.M. Stencel, Raman Spectroscopy for Catalysis, Van Norstrand Reinhold Catalysis Series, New York, 1990.
[29] J.C. Carter, P.K. Khulbe, J. Gray, J.W. Van Zee, S. Michael Angel, Anal. Chim. Acta 514 (2004) 241–245.
[30] M. Fournier, C. Louis, M. Che, P. Chaquin, D. Masure, J. Catal. 119 (1989) 400–414.
[31] A.B. Lever, Inorganic electronic spectroscopy, 2nd edition, Studies in Physical Theoretical Chemistry, vol. 33, Elsevier, Amsterdam, 1984, pp. 507–711.
[32] F. Iova, A. Trutia, Opt. Mater. 13 (2000) 455–458.
[33] C. Lepetit, M. Che, J. Phys. Chem. 100 (1996) 3137–3143.
[34] S.-C. Chang, M.A. Leugers, R.B. Simon, J. Phys. Chem. 96 (1992) 10358–10365.
[35] Y. Sendota, Y. Ono, T. Keii, J. Catal. 39 (1975) 357–362.
[36] M.L. Jacono, M. Sachiavello, A. Cimino, J. Phys. Chem. 75 (1971) 1044–1050.